

A Direct Comparison of the MM-GB/SA Scoring Procedure and Free-Energy Perturbation Calculations Using Carbonic Anhydrase as a Test Case: Strengths and Pitfalls of Each Approach

Cristiano R. W. Guimaraes*

Worldwide Medicinal Chemistry Department, Pfizer Inc., 558 Eastern Point Rd, Groton, Connecticut 06340, United States

ABSTRACT: MM-GB/SA scoring and free energy perturbation (FEP) calculations have emerged as reliable methodologies to understand structural and energetic relationships to binding. In spite of successful applications to elucidate the structure–activity relationships for few pairs of ligands, the reality is that the performance of FEP calculations has rarely been tested for more than a handful of compounds. In this work, a series of 13 benzene sulfonamide inhibitors of carbonic anhydrase with binding free energies determined by isothermal titration calorimetry was selected as a test case. R^2 values of 0.70, 0.71, and 0.49 with the experiment were obtained with MM-GB/SA and FEP simulations run with MCPRO+ and Desmond, respectively. All methods work well, but the results obtained with Desmond are inferior to MM-GB/SA and MCPRO+. The main contrast between the methods is the level of sampling, ranging from full to restricted flexibility to single conformation for the complexes in Desmond, MCPRO+, and MM-GB/SA, respectively. The current and historical results obtained with MM-GB/SA qualify this approach as a more attractive alternative for rank-ordering; it can achieve equivalent or superior predictive accuracy and handle more structurally dissimilar ligands at a fraction of the computational cost of the rigorous free-energy methods. As for the large theoretical dynamic range for the binding energies, that seems to be a direct result of the degree of sampling in the simulations since MCPRO+ as well as MM-GB/SA are plagued by this. Van't Hoff analysis for selected pairs of ligands suggests that the wider scoring spread is not only affected by missing entropic contributions due to restricted sampling but also exaggerated enthalpic separation between the weak and potent compounds caused by diminished shielding of electrostatic interactions, thermal effects, and protein relaxation/strain.

INTRODUCTION

Computational methodologies to understand structural and energetic relationships to binding vary in speed and accuracy. Molecular dynamics (MD) and Monte Carlo (MC) simulations coupled with free-energy perturbation (FEP) or thermodynamic integration (TI) calculations are considered the reference computational approaches when it comes to estimating relative binding affinities.^{1–5} Although the FEP and TI equations are exact, the results are plagued by (i) force fields that incompletely or incorrectly describe the protein, the ligand, and their interactions; (ii) limited sampling of the phase space; and (iii) challenges in accurately taking into account changes in hydration.^{6–8} In spite of successful applications to elucidate the structure–activity relationships for a few pairs of ligands in a congeneric series, the reality is that the performance of FEP and TI calculations has rarely been tested for more than a handful of compounds due to the high computational cost, with a few exceptions that are noteworthy.⁹

The combination of molecular mechanics and the Poisson–Boltzmann continuum solvation to compute binding free energies was pioneered by Kollman and Kuhn.¹⁰ The encouraging results obtained with this methodology inspired several authors to use molecular-mechanics-based scoring functions with the generalized Born model¹¹ as the implicit solvent (MM-GB/SA) in the rescoring of docking poses. When compared to docking scoring functions, the MM-GB/SA procedure provides improved enrichment in the virtual screening of databases and better correlation between calculated binding affinities and experimental data.¹² The MM-GB/SA rescoring method, however, performs poorly in some cases, suggesting that success through its application may be system- and/or protocol-dependent.¹³

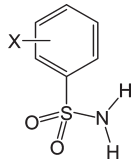
We investigated the performance of our own flavor of MM-GB/SA when rescoring docking poses of congeneric series for the pharmaceutically relevant targets CDK2, Factor Xa, Thrombin, and HIV-RT.¹⁴ The correlation with experimental results obtained with the physics-based scoring was far superior to the one obtained with the Glide XP scoring function.¹⁵ More recently, we addressed the poor estimation of protein desolvation provided by the GB/SA solvation model;¹⁶ replacing this term with the free energy associated with displacing binding-site waters upon ligand binding estimated by the WaterMap method,¹⁷ which treats the solvent explicitly, provides superior results. However, the improvement is modest over results obtained with the MM-GB/SA version that excludes the protein GB/SA desolvation term. This is apparently due to the high correlation between the free energy liberation of the displaced solvent and the protein–ligand van der Waals interactions, which in turn may be interpretable as estimates of the hydrophobic effect and hydrophobic-like interactions, respectively.

The remarkable results obtained with MM-GB/SA^{14,16} warrant a head-to-head comparison with the more rigorous but computationally intensive FEP and TI methodologies to address whether the approximate free-energy method provides a more attractive alternative for rank-ordering. Although the MM-GB/SA approach handles more structurally dissimilar ligands and provides results at a fraction of the computational cost than FEP and TI, it is not clear if it can achieve equivalent predictive accuracy. To accomplish that, a subset with 13 ligands of a series of benzene sulfonamide (BSA) inhibitors of carbonic anhydrase

Received: April 8, 2011

Published: June 02, 2011

Table 1. Isothermal Titration Calorimetry (ITC) Data for the Binding between the Human Carbonic Anhydrase (hCAII) and a Series of Benzene Sulfonamide (BSA) Inhibitors^a



| R | ΔG_{bind}^b | pK_a^b | IP ^c | $c\Delta G_{\text{bind}}^d$ |
|-------------------|----------------------------|----------|-----------------|-----------------------------|
| H | -8.3 | 10.1 | 3.5 | -11.8 |
| 2-F | -8.8 | 9.6 | 2.9 | -11.7 |
| 3-F | -9.4 | 9.7 | 3.0 | -12.4 |
| 4-F | -8.4 | 10.0 | 3.4 | -11.8 |
| 2-Cl | -8.1 | 9.5 | 2.7 | -10.8 |
| 3-Cl | -8.5 | 9.5 | 2.7 | -11.2 |
| 4-Cl | -9.3 | 9.9 | 3.3 | -12.6 |
| 2-CH ₃ | -7.9 | 10.0 | 3.4 | -11.3 |
| 3-CH ₃ | -8.1 | 10.2 | 3.7 | -11.8 |
| 4-CH ₃ | -8.7 | 10.3 | 3.8 | -12.5 |
| 2-NH ₂ | -8.2 | 10.0 | 3.4 | -11.6 |
| 3-NH ₂ | -8.1 | 10.0 | 3.4 | -11.5 |
| 4-NH ₂ | -7.8 | 10.5 | 4.1 | -11.9 |

^a Energy values are in kcal/mol. ^b Ref 18. ^c Ionization penalty \rightarrow IP = $RT \ln(1 + 10^{(pK_a - pH)})$. ^d $c\Delta G_{\text{bind}} = \Delta G_{\text{bind}} - RT \ln(1 + 10^{(pK_a - pH)})$.

with binding free energies determined by isothermal titration calorimetry (ITC) was selected (Table 1).¹⁸ This subset is attractive since the degree of similarity is ideal for the FEP and TI techniques; it involves “walks” of typical one-heavy atom substituents around a benzene ring. A negative aspect of this series is the narrow dynamic range for the experimental binding free energies (Table 1).

In this work, relative binding free energies ($\Delta\Delta G_{\text{bind}}$) for the BSA series were calculated by MM-GB/SA and FEP and compared to the free energies obtained with ITC; the original MM-GB/SA implementation¹⁴ and the implementation augmented by Watermap¹⁶ were used. In addition, the large dynamic range observed in the MM-GB/SA scoring compared to the experimental range was revisited. To accomplish that, FEP simulations with different degrees of sampling were performed since this problem resides in the use of a single, relaxed structure for the complex in MM-GB/SA.¹⁶ Finally, a computational Van't Hoff analysis was conducted for selected pairs of ligands to further dissect the origin of the large dynamic range, e.g., enthalpic, entropic, or a combination of both.

METHODS

System. The crystal structure between the human carbonic anhydrase (hCAII) and the unsubstituted BSA analog was used (PDB ID: 2WEJ; Figure 1).¹⁸ The starting structure was refined through a series of restrained, partial minimizations using the OPLS_2005 force field.^{19,20} A view of the binding site reveals that the zinc ion (Zn^{2+}) is coordinated to three histidine residues and the deprotonated nitrogen of the sulfonamide group. This group is not particularly acidic, as shown by the measured pK_a 's in Table 1, so the ITC ΔG_{bind} values have to be corrected by the application of eq 1. The second term represents the ionization penalty (IP) to charge a molecule whose pK_a value is greater than the pH of the

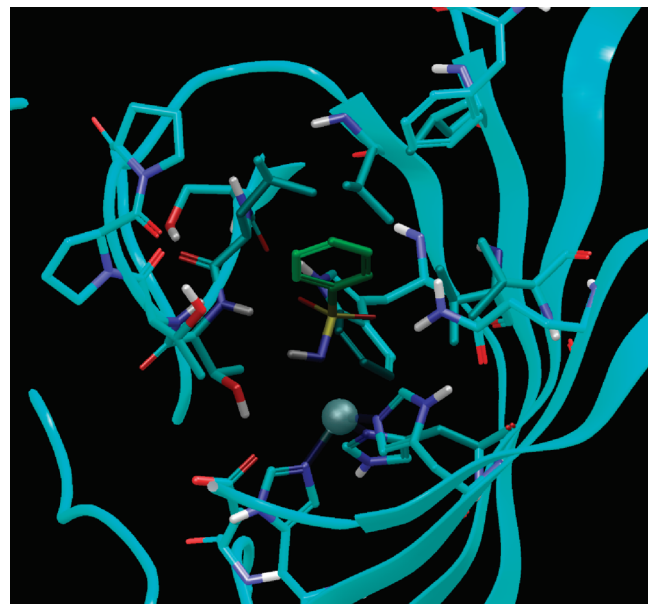


Figure 1. The crystal structure between the human carbonic anhydrase (hCAII) and the unsubstituted benzene sulfonamide inhibitor (PDB ID: 2WEJ).

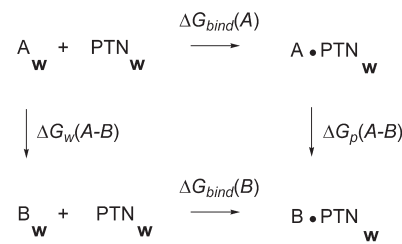


Figure 2. Thermodynamic cycle used for the calculation of relative binding free energies ($\Delta\Delta G_{\text{bind}}$). ΔG_{bind} is the absolute binding free energy. ΔG_w and ΔG_p are the free energy changes for the transformation of ligand A into B in water and in the solvated complex.

experiment, which was set to 7.5. This correction is necessary since the simulations were carried out for the inhibitors in their deprotonated state.

$$c\Delta G_{\text{bind}} = \Delta G_{\text{bind}} - RT \ln(1 + 10^{(pK_a - pH)}) \quad (1)$$

FEP Simulations. Figure 2 illustrates the thermodynamic cycle used to calculate free energy changes.²¹ Since free energy is a thermodynamic state function, eq 2 can be derived from the cycle and used to calculate $\Delta\Delta G_{\text{bind}}$, where A and B are any two analogs, ΔG_{bind} is the absolute binding free energy, and $\Delta G_w(A \rightarrow B)$ and $\Delta G_p(A \rightarrow B)$ are the free energies associated with the transformation of A into B in water and in the solvated complex, computed by the FEP method.

$$\begin{aligned} \Delta\Delta G_{\text{bind}} &= \Delta G_{\text{bind}}(B) - \Delta G_{\text{bind}}(A) \\ &= \Delta G_p(A \rightarrow B) - \Delta G_w(A \rightarrow B) \end{aligned} \quad (2)$$

FEP simulations were performed for the compounds in Table 1 using the unsubstituted analog as the reference state. The MC and

Table 2. λ Schedules Used in the FEP Simulations Run with Desmond

| state | 1 | 2 | 3 | 4 | 5 | 6 | 7 | 8 | 9 | 10 | 11 | 12 |
|-----------|------|------|------|------|------|------|------|------|------|------|------|------|
| VDW A | 1.00 | 1.00 | 1.00 | 1.00 | 1.00 | 0.67 | 0.46 | 0.33 | 0.25 | 0.19 | 0.12 | 0.00 |
| VDW B | 0.00 | 0.12 | 0.19 | 0.25 | 0.33 | 0.46 | 0.67 | 1.00 | 1.00 | 1.00 | 1.00 | 1.00 |
| Coulomb A | 1.00 | 0.75 | 0.50 | 0.25 | 0.00 | 0.00 | 0.00 | 0.00 | 0.00 | 0.00 | 0.00 | 0.00 |
| Coulomb B | 0.00 | 0.00 | 0.00 | 0.00 | 0.00 | 0.00 | 0.00 | 0.00 | 0.25 | 0.50 | 0.75 | 1.00 |
| Bonded A | 1.00 | 0.91 | 0.82 | 0.73 | 0.64 | 0.55 | 0.45 | 0.36 | 0.27 | 0.18 | 0.09 | 0.00 |
| Bonded B | 0.00 | 0.09 | 0.18 | 0.27 | 0.36 | 0.45 | 0.55 | 0.64 | 0.73 | 0.82 | 0.91 | 1.00 |

MD sampling techniques as implemented in MCPRO+ and Desmond were used.^{22,23} No effort has been made to make the two codes as comparable as possible; the recommended options for each piece of software were used. The goal was to evaluate the performance of each FEP method from a nonexpert user's point of view. However, it should be noted that the default settings have been carefully determined by the experts in the field. These settings were obtained with not only accuracy but also computational time in mind, so that a $\Delta\Delta G_{\text{bind}}$ prediction between two compounds can be provided within 1 to 2 days when multi-CPU processing is available.

The degrees of freedom for the protein backbone atoms were not sampled in the MC simulations. The only protein degrees of freedom allowed to vary during the simulation were the bond angles and dihedral angles for the side chains of residues with any atom within 10 Å from the ligands. The ligands, however, are fully flexible in the MC simulations. In the MD simulations, all degrees of freedom are sampled, except for the bonds that are formed by a heavy atom and a hydrogen atom; those were constrained by the Shake algorithm.²⁴

Charge neutrality for the protein systems in MCPRO+ was imposed by assigning normal protonation states at physiological pH to basic and acidic residues near the active site and making the adjustments for neutrality to the most distant residues. The complexes and the ligands in solution were solvated with a 22-Å-radius water cap. A half-harmonic potential with a force constant of 1.5 kcal/mol·Å² was applied to water molecules at distances greater than 22 Å from the center of the system to discourage evaporation. Residue-based nonbonded cutoffs of 10 Å were employed. In Desmond, charge neutrality was achieved by the addition of a minimal concentration of ions. The complexes and the ligands in solution were placed in a cubic box using periodic boundary conditions with buffer regions of 5 Å and 10 Å, respectively. Short-range van der Waals (VDW) and near electrostatic nonbonded interactions were computed by summing them over all pairs within 9 Å of each other. Far electrostatic interactions were computed using the smooth particle mesh Ewald method.²⁵

The A→B transformations in MCPRO+ were performed using the single topology approach by melding the force field parameters for bond lengths, bond angles, torsions, and nonbonded interactions. In order to keep the number of atoms constant, dummy atoms were introduced for hydrogens that exist in one state and have no counterpart in the other. Desmond performs the transformations using the dual topology approach, where both ligands A and B are simultaneously simulated, but they do not interact with each other.⁷ The free energy changes in MCPRO+ and Desmond employed the double wide sampling and the Bennett acceptance ratio²⁶ methods, respectively. Other important differences between MCPRO+ and Desmond reside in the use by the latter of a softcore potential for VDW interactions and a decoupled λ schedule. The softcore potential is introduced to avoid the so-called van der Waals end point problems when an atom is being created or

annihilated.²⁷ As for the λ schedule, the force field parameters are mutated concomitantly in MCPRO+ using 20 windows with λ values evenly distributed between 0 and 1. In Desmond, the bonded, VDW, and Coulomb interactions for ligands A and B have independent λ schedules, as shown in Table 2.

The A→B transformations were executed at 298 K. The Van't Hoff plots for selected pairs of ligands were obtained by also running the transformations at 298 ± 30 K, the reference temperature. In MCPRO+, initial relaxation of the solvent was performed for 5×10^6 configurations, followed by 10×10^6 configurations of full equilibration and 20×10^6 configurations of data collection for each window in water or in the complex. Established procedures including Metropolis and preferential sampling were employed. Attempted moves of the ligands in water occurred every 60 configurations, while in the complex attempted moves of the protein systems and ligand analogs occurred every 10 and 60 configurations, respectively. In Desmond, the complex and the ligand went through a relaxation process that includes two energy minimizations, with and without solute restraints, followed by four short MD simulations, the first at 10 K in the NVT ensemble, the second also at 10 K but in the NPT ensemble, and the last two at 298 K in the NPT ensemble. The production simulation, also in the NPT ensemble, was run for 0.6 ns for each λ window. The temperature and pressure in the MD simulations were controlled by the Berendsen thermostat and barostat algorithms.²⁸ The TIP4P²⁹ and SPC water models³⁰ were used in MCPRO+ and Desmond, respectively, while the OPLS_2005 force field^{19,20} was employed for both.

To account for the two possible orientations in the binding site for the unsymmetrical ligands, where substituents at the 2 and 3 positions of the phenyl ring may be oriented to the left (L) or right (R) using the pose in Figure 1 as a reference, the free energies of binding of each orientation, $\Delta\Delta G_{\text{bind}}^{\text{L}}$ and $\Delta\Delta G_{\text{bind}}^{\text{R}}$, were combined to produce an overall $\Delta\Delta G_{\text{bind}}$ using eq 3, where R is the ideal gas constant and T is the temperature. The second term in eq 3 penalizes the computed free energies of binding of the unsymmetrical ligands by $RT \ln 2$ because they are relative to the unsubstituted, symmetrical ligand. Thus, when the relative free energies of binding of the two orientations differ by greater than ca. 2 kcal/mol, the free energy of binding is essentially that of the more favorable orientation plus $RT \ln 2$. Alternatively, if the relative free energies of binding of the two orientations are the same, the $RT \ln 2$ penalty is removed.^{9b}

$$\Delta\Delta G_{\text{bind}} = -RT \ln \left[\exp \left(-\frac{\Delta\Delta G_{\text{bind}}^{\text{L}}}{RT} \right) + \exp \left(-\frac{\Delta\Delta G_{\text{bind}}^{\text{R}}}{RT} \right) \right] + RT \ln 2 \quad (3)$$

MM-GB/SA Rescoring. In our implementation of the MM-GB/SA rescoring (Figure 3), described in detail in refs 14 and 16,

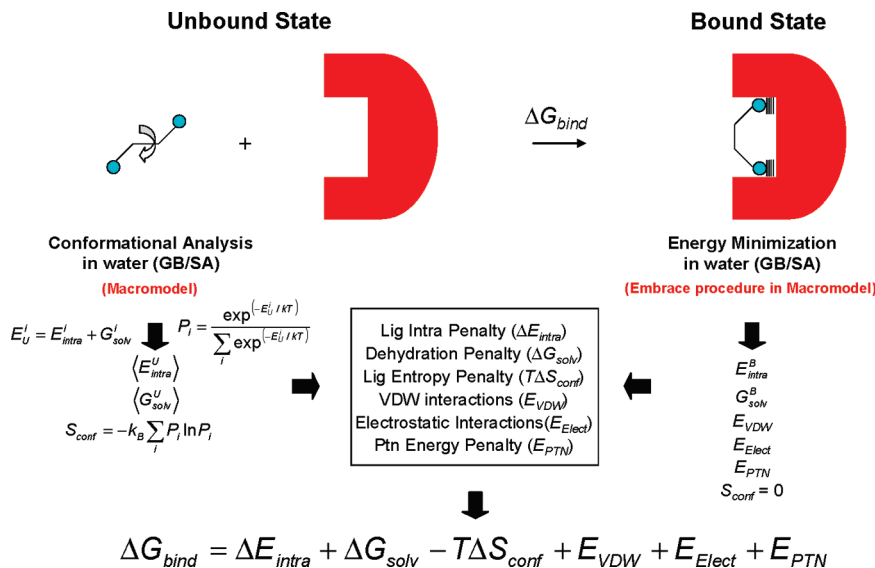


Figure 3. Schematic representation of the MM-GB/SA rescoring procedure with no protein desolvation term.

a conformational search for the inhibitors in the unbound state and energy minimization for the complexes using OPLS_2005 and GB/SA within MacroModel³¹ are performed. All conformers within 5.0 kcal/mol from the lowest energy conformer were retained. Assuming a Boltzmann distribution, the probability for each conformer (P_i) was calculated and used to compute the Boltzmann-averaged intramolecular energy and solvation free energy in the unbound state for each compound. The conformational entropies (S_{conf}) were computed from the probabilities using eq 4, where k_B is the Boltzmann constant.

$$S_{\text{conf}} = -k_B \sum_{i=1}^n p_i \ln p_i \quad (4)$$

To better account for the protein flexibility, each inhibitor was energy-minimized in the bound state. The preferred orientations for the unsymmetrical ligands were determined by the FEP simulations. In the energy minimization, no constraints were applied to residues within 5 Å from the center of the system. A second shell of 3 Å around the first shell was defined and constraints of 50 kcal/mol·Å² applied to the residues therein. The remaining residues were held fixed. After the energy minimization step, the protein energy (E_{PTN}) values for all complexes were extracted. This term describes the protein deformation or strain imposed by each ligand. Besides E_{PTN} , the energy-minimized structures for the complexes provided the intramolecular energies and solvation free energies for the ligands in the protein environment and the protein–ligand intermolecular van der Waals (E_{VDW}) and electrostatic (E_{Elect}) interaction energies. In the bound state, it was assumed that there was only one conformation accessible to each ligand; its conformational entropy is therefore zero. In this manner, ΔG_{bind} estimated by MM-GB/SA was calculated as shown in eq 5.

$$\Delta G_{\text{bind}} = \Delta E_{\text{intra}} + \Delta G_{\text{solv}} - T\Delta S_{\text{conf}} + E_{\text{VDW}} + E_{\text{Elect}} + E_{\text{PTN}} \quad (5)$$

In eq 5, ΔE_{intra} and ΔG_{solv} are the intramolecular strain and desolvation penalty for each ligand upon binding. Similarly, $-T\Delta S_{\text{conf}}$ is the ligand conformational entropy penalty, multiplied by the temperature to convert it into energy. The final ranking was obtained by

calculating relative binding energies, $\Delta\Delta G_{\text{bind}}$, using the top-scoring inhibitor as a reference.

In our MM-GB/SA implementation, although solvent effects are included in the protein–ligand complex geometry optimization using GB/SA, the protein desolvation term calculated by the continuum model ($\Delta G_{\text{solv}}^{\text{ptn}}$), defined as illustrated in Figure 4, is generally excluded from the scoring since it deteriorates the correlation with experimental data.^{14,16} The solvent shielding of protein–ligand electrostatic interactions estimated by the GB model (E_{GB}) as well as rotational, translational, and vibrational entropy changes for the ligand upon binding using the rigid-rotor harmonic oscillator (RRHO) approximation are also excluded, as they have no significant impact on the MM-GB/SA results. Here, we decided to investigate the impact of these contributions on the results for the BSA series in hCAII since the degree of similarity for the ligands (Table 1) is greater than the typical congeneric series previously evaluated.^{14,16}

WaterMap. In WaterMap, the reference state consists of an assumed-to-pre-exist cavity in solution formed to accommodate the ligand. In order to accommodate ligand binding, the binding site waters get displaced to the cavity in solution, leaving a cavity of identical size and shape in the protein (Figure 5). The displaced-solvent functional in WaterMap represents an attempt to estimate the free energy liberation (ΔG_{WM}) for the binding site waters into bulk solution upon cavity transfer between the two environments. This functional depends on the degree of overlap between the ligand heavy atoms and the hydration sites and the energetics of the waters that are displaced. Specifically, the functional considers that a water molecule is completely displaced, and therefore its full energy is liberated when the distance between the hydration site center and the ligand heavy atom approaches zero. The energy of hydration site displacement then decreases linearly to a value of zero when the distance between the two atoms is equal to 80% of the sum of their VDW radii, beyond which there is no displacement. Multiple ligand atoms may contribute to the displacement of a given hydration site; however, these contributions cease once total displacement is achieved. The *ab initio* form of the displaced-solvent functional as described by Abel and co-workers was employed in this

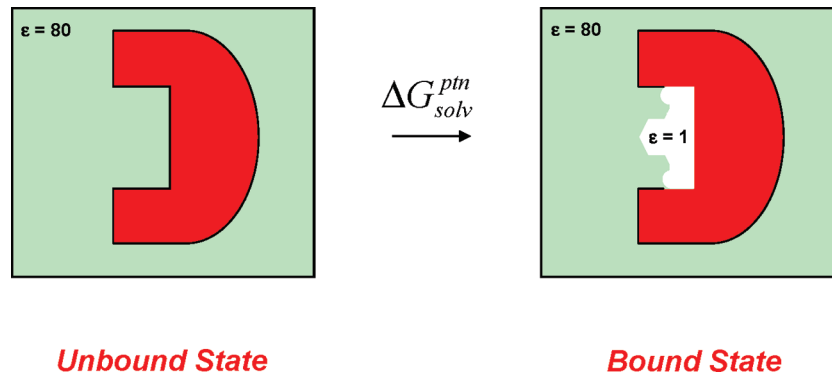


Figure 4. Schematic representation of the protein desolvation term ($\Delta G_{\text{solv}}^{\text{ptn}}$) described by GB/SA. The white area represents the vacuum region in the protein binding site that will be occupied by a ligand of that shape and size.

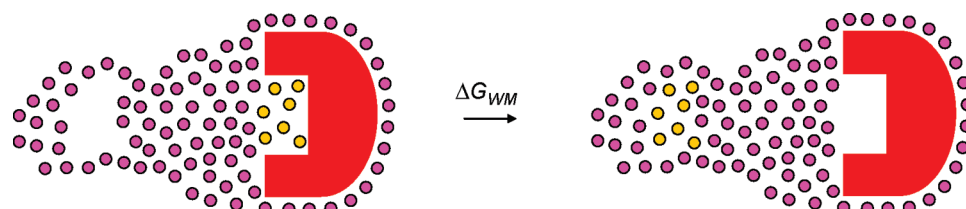


Figure 5. Schematic representation of the process simulated by WaterMap. The white area represents the cavity in the bulk that is transferred to the protein binding site. The orange dots represent the binding site waters that get displaced into the bulk solution. WaterMap estimates the free energy liberation (ΔG_{WM}) for the displaced waters.

work.¹⁷ The thermodynamic and structural properties of theoretical water molecules in the binding sites of hCAII were obtained from MD simulations of 10 ns each using WaterMap.³² The protein heavy atoms were harmonically restrained to their starting coordinates. The ligands were scored using the poses extracted from the energy-minimized complexes.

RESULTS AND DISCUSSION

MM-GB/SA Scoring. The orientations for the unsymmetrical ligands were determined by the FEP simulations. MCPRO+ and Desmond agree in all cases for the 2- and 3-substituted analogs. Specifically, the 2-F, 2-NH₂, and 3-NH₂ analogs adopt the L orientation, where they face a more polar region of the binding site and hydrogen bonds may be established. The 3-F, 2-Cl, 3-Cl, 2-CH₃, and 3-CH₃ analogs adopt the R orientation; in this orientation, they point the more apolar substituents toward the hydrophobic wall of the deep conical-cleft-binding site of hCAII. The FEP predictions for 2-F, 3-F, and 2-Cl agree with the orientations observed in their crystal structures.¹⁸

Table 3 summarizes the impact of different contributions on the results obtained with the MM-GB/SA scoring procedure. The correlation (R^2) between the $\Delta \Delta G_{\text{bind}}$ values calculated by eq 5 and the experimental data, corrected as shown in eq 1, is 0.51. The addition of rotational, translational, and vibrational entropy changes for the ligand upon binding using the RRHO approximation plus the E_{GB} term, the solvent shielding of protein–ligand electrostatic interactions, marginally improves the results. Interestingly in this case, the protein desolvation term, $\Delta G_{\text{solv}}^{\text{ptn}}$, improves the correlation with experimental results, as can be seen when rows 2 and 3 in Table 3 are compared to 4 and 6, respectively. This term is generally excluded from our

Table 3. Correlation (R^2) between the Experimental Data, Corrected As Shown in eq 1, and the MM-GB/SA Scoring Approach Including Different Contributions

| | R^2 |
|---|-------|
| MM-GB/SA ^a | 0.51 |
| MM-GB/SA + RRHO ^b | 0.53 |
| MM-GB/SA + RRHO + E_{GB}^{c} | 0.54 |
| MM-GB/SA + RRHO + $\Delta G_{\text{solv}}^{\text{ptn}}\text{d}$ | 0.60 |
| MM-GB/SA + RRHO + $\Delta G_{\text{WM}}^{\text{e}}$ | 0.59 |
| MM-GB/SA + RRHO + $E_{\text{GB}} + \Delta G_{\text{solv}}^{\text{ptn}}$ | 0.60 |
| MM-GB/SA + RRHO + $E_{\text{GB}} + \Delta G_{\text{WM}}$ | 0.53 |

^a MM-GB/SA scoring using eq 5. ^b Including rotational, translational, and vibrational entropy changes for the ligand upon binding as estimated by the rigid-rotor harmonic oscillator (RRHO) approximation. ^c Including the solvent shielding of the protein–ligand electrostatic interactions (E_{GB}). ^d Including the protein GB/SA desolvation penalty upon binding ($\Delta G_{\text{solv}}^{\text{ptn}}$). ^e Including the free energy liberation for the binding site waters into bulk solution (ΔG_{WM}).

scoring procedure, as it deteriorates the results.^{14,16} One possible explanation is that errors in the continuum solvation model are more likely to be canceled when there is a higher degree of similarity within the series being scored, which is the case with the BSA series.

The WaterMap method alone does not perform particularly well with an R^2 value of 0.28. This contrasts with results obtained for FactorXa and CDK2, where R^2 values of 0.71 and 0.68 were obtained.¹⁶ This is not surprising as the ligands in the BSA series are much more similar in size, indicating that the affinity differences are driven by contributions other than the hydrophobic effect. For example, WaterMap makes no differentiation between

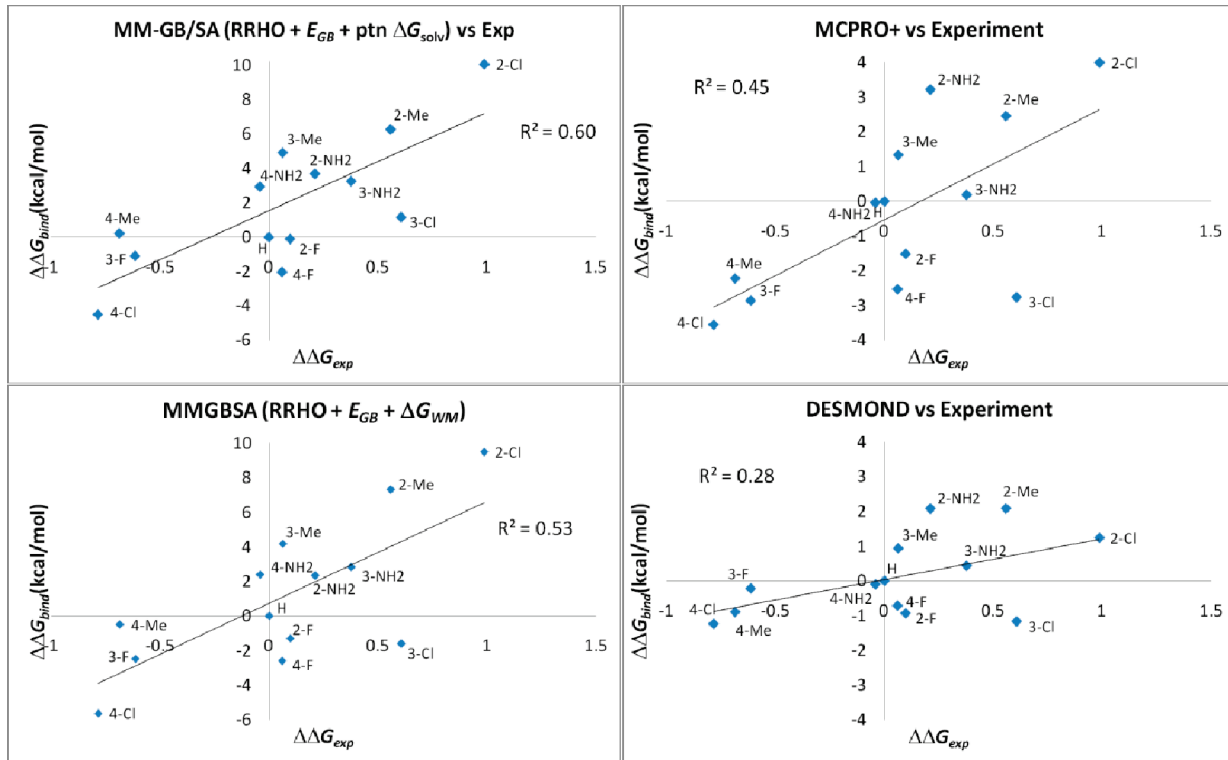


Figure 6. Correlation between isothermal titration calorimetry $\Delta\Delta G_{\text{bind}}$ values for the human carbonic anhydrase inhibitors, corrected as shown in eq 1, and MM-GB/SA ($\text{MM-GB/SA} + \text{RRHO} + E_{\text{GB}} + \Delta G_{\text{solv}}^{\text{ptn}}$), MM-GB/SA combined with WaterMap ($\text{MM-GB/SA} + \text{RRHO} + E_{\text{GB}} + \Delta G_{\text{WM}}$), and FEP simulations run with MCPRO+ and Desmond.

the 2-Cl and 2-CH₃ derivatives, as they have identical binding modes and displace essentially the same water molecules upon binding; the $c\Delta G_{\text{bind}}$ values in Table 1 for these analogs, however, are -10.8 and -11.3 kcal/mol, respectively. The same is true for the 4-substituted subset with $c\Delta G_{\text{bind}}$ values of -11.3 , -12.6 , -12.5 , and -11.9 kcal/mol for F, Cl, CH₃, and NH₂; WaterMap provides identical scores to all of them. In spite of that, adding the free energy liberation for the displaced solvent, ΔG_{WM} , to the MM-GB/SA score is either beneficial, when the E_{GB} term is not included (rows 2 and 5), or neutral, in the case that this term is included (rows 3 and 7). Overall, our previous accounts^{14,16} and the results in Table 3 suggest that the terms in eq 5 contain most of the information needed to describe the binding process for congeneric series and that the addition of other contributions provides only incremental improvements to the scoring equation.

MM-GB/SA Scoring versus FEP Simulations. Figure 6 illustrates the correlations with the experimental results obtained with MCPRO+, Desmond, and MM-GB/SA. In the case of MM-GB/SA, the analysis is focused on the equation that includes the RRHO, E_{GB} , and $\Delta G_{\text{solv}}^{\text{ptn}}$ contributions, as it provides the best correlation with the ITC data. The scoring version where $\Delta G_{\text{solv}}^{\text{ptn}}$ is substituted by ΔG_{WM} is also included for comparison.

Superior correlation is obtained with the MM-GB/SA methods, followed by MCPRO+ and Desmond FEP simulations. This cannot necessarily be attributed to a lack of convergence in the MCPRO+ and Desmond simulations, as the calculated values obtained with different levels of sampling agree with each other (Figure 7). Desmond and MCPRO+ $\Delta\Delta G_{\text{bind}}$ values are highly correlated with an R^2 of 0.85. Both FEP methods, in particular MCPRO+, are also correlated with the results provided by the MM-GB/SA method, in spite of the particularities of each approach,

such as explicit versus implicit solvent treatments, which could lead to discrepancies in the free-energy values; R^2 values of 0.81 and 0.61 are observed when the MM-GB/SA scores are plotted against MCPRO+ and Desmond $\Delta\Delta G_{\text{bind}}$ values, respectively. It is interesting to see that MCPRO+, with restricted sampling, behaves almost like an interpolation between two methodological extremes, characterized by MM-GB/SA where a single, energy-minimized structure for each complex is used and Desmond where full sampling is performed.

The fact that the calculated $\Delta\Delta G_{\text{bind}}$ values obtained with the different methods are in closer agreement with each other than they are with the experimental data points to the existence of common outliers. A close inspection of Figure 6 reveals that the 3-Cl derivative is an outlier for all methods, in particular the ones where explicit solvation is used, indicating that the problem with this compound might lie in inaccuracies when simulating its change in hydration upon binding or a more fundamental problem with the energy function or with the experimental data. When the 3-Cl analog is removed, the correlation improves for all methods (Figure 8); R^2 values change from 0.60, 0.53, 0.45, and 0.28 to 0.70, 0.72, 0.71, and 0.49 for MM-GB/SA, MM-GB/SA combined with WaterMap, and FEP simulations run with MCPRO+ and Desmond, respectively. All methods work well, especially considering the narrow experimental dynamic range of 1.8 kcal/mol, but the results obtained with Desmond are inferior to MM-GB/SA and MCPRO+. It is possible that the full flexibility for the systems in Desmond actually adds more noise than information due to the sampling of nonrelevant conformations and/or sampling of relevant conformations that are not adequately weighted in the simulations. The restricted sampling in MCPRO+, besides reducing computational cost, aims at

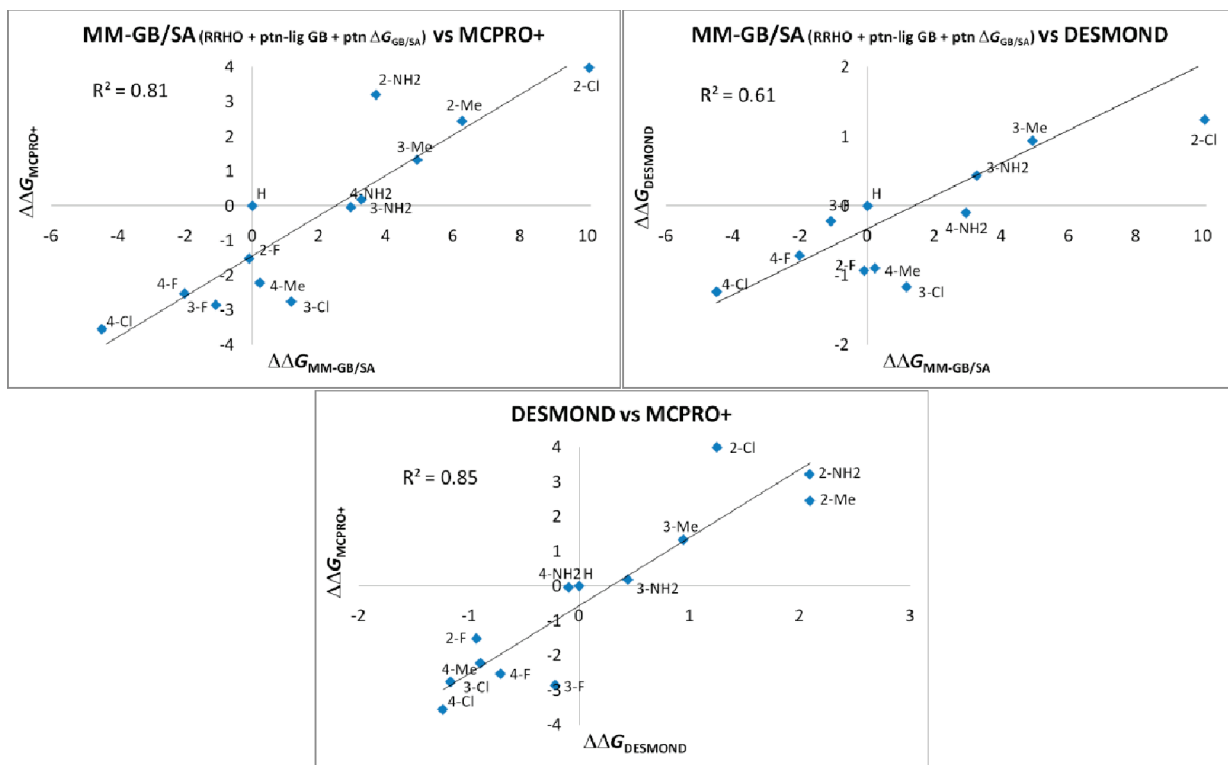


Figure 7. Correlation among MM-GB/SA (MM-GB/SA + RRHO + E_{GB} + $\Delta G_{\text{solv}}^{\text{ptn}}$) and FEP simulations run with MCPRO+ and Desmond.

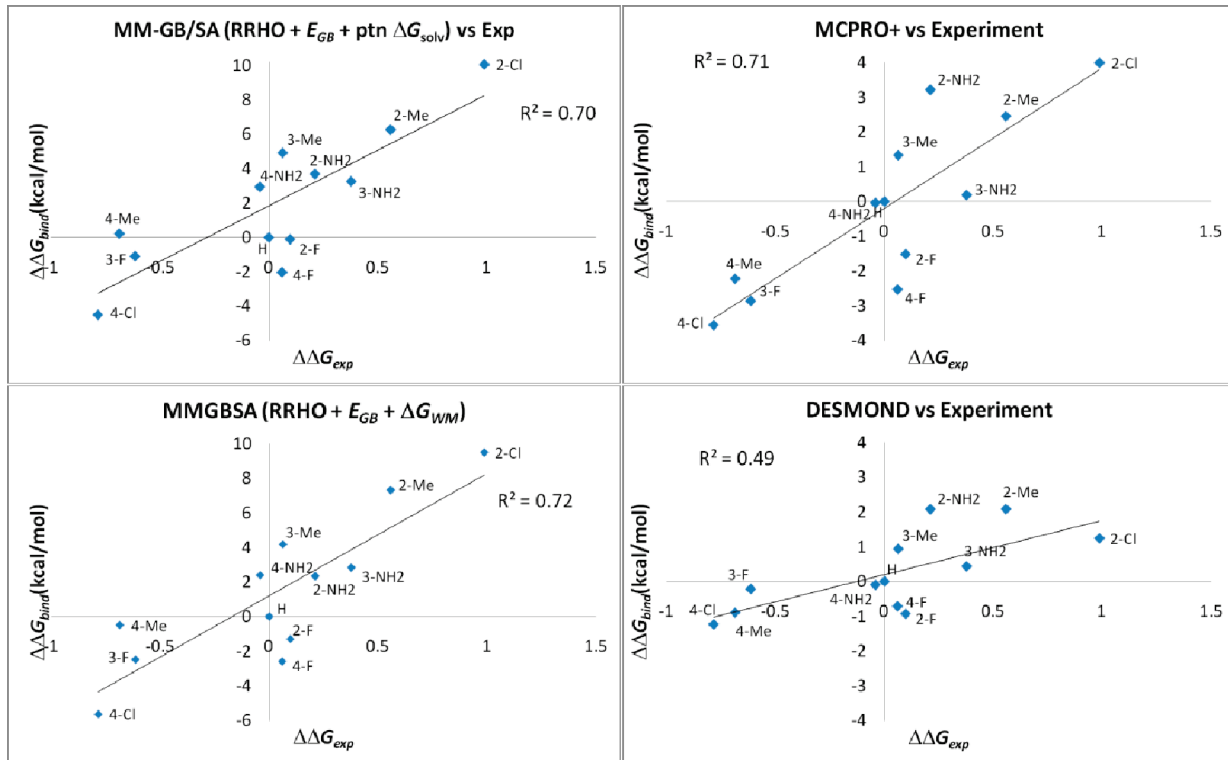


Figure 8. Correlation between isothermal titration calorimetry $\Delta \Delta G_{\text{bind}}$ values for the human carbonic anhydrase inhibitors, corrected as shown in eq 1, and MM-GB/SA (MM-GB/SA + RRHO + E_{GB} + $\Delta G_{\text{solv}}^{\text{ptn}}$), MM-GB/SA combined with WaterMap (MM-GB/SA + RRHO + E_{GB} + ΔG_{WM}), and FEP simulations run with MCPRO+ and Desmond. The 3-Cl analog is removed from the plots.

focusing the MC simulations on crystal-structure-like conformations for the complexes as the protein backbone atoms are

untouched during the MC simulations. The assumption in MM-GB/SA, that one conformation captures the essence of

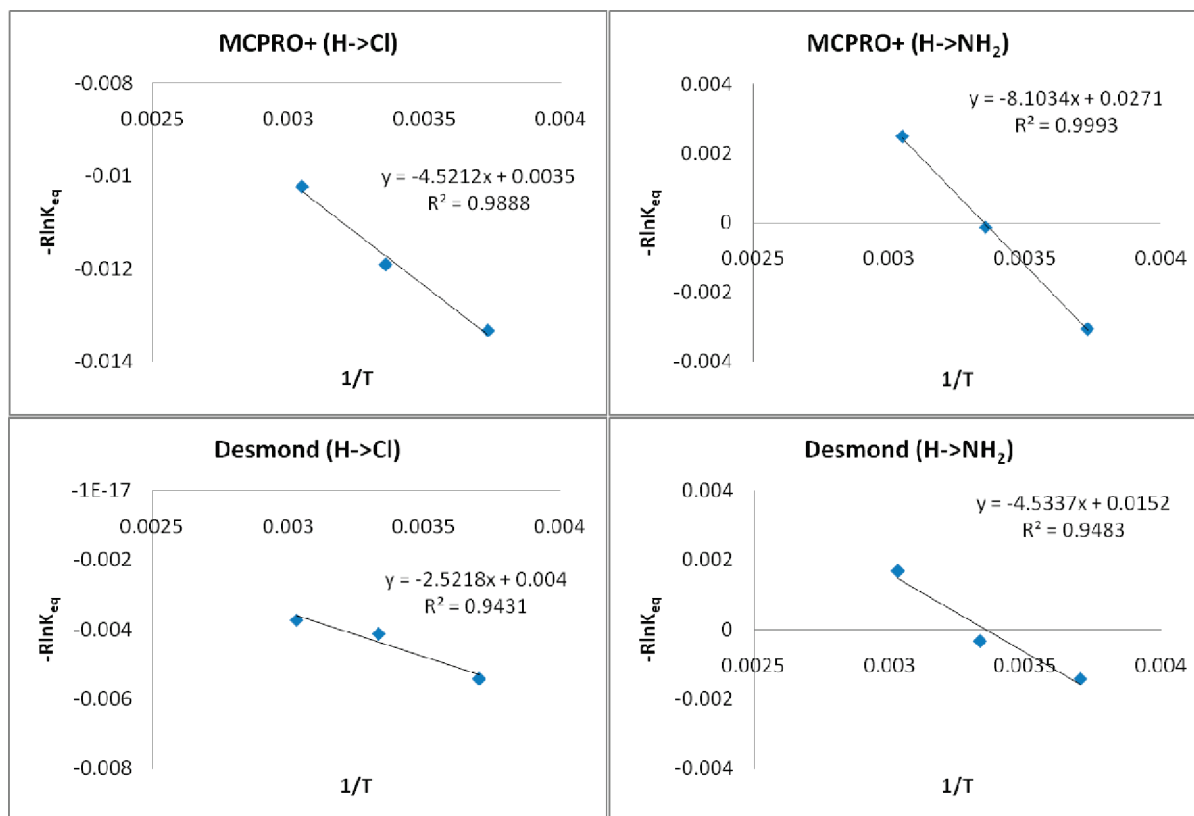


Figure 9. Van't Hoff plots obtained with MCPRO+ (top) and Desmond (bottom) for the $H \rightarrow 4\text{-Cl}$ and $H \rightarrow 4\text{-NH}_2$ pairs.

the binding process, is an even more drastic restriction. However, on the basis of the present and historical results,^{14,16} it seems to be reasonable, at least for congeneric series. The results obtained with MM-GB/SA even qualify this approach as a more attractive alternative for rank-ordering; it can achieve equivalent or superior predictive accuracy and handle more structurally dissimilar ligands at a fraction of the computational cost of the rigorous free-energy methods.

Large Dynamic Range in MM-GB/SA: Comparison with FEP Results. Figure 6 shows a large dynamic range for the MM-GB/SA method (~ 15 kcal/mol) compared to the experimental range (~ 1.8 kcal/mol). This is a phenomenon typically observed in MM-GB/SA calculations,^{14,16} and it is not particular of the case studied in this work. As discussed previously,¹⁶ the large dynamic range observed in the MM-GB/SA scoring could have its origin in several effects, some enthalpic and others entropic in nature. In the former, it is possible that the wider scoring spread is due to the application of a protein dielectric constant of 1 in a model where protein motions and polarization are not taken into account. Therefore, electrostatic interactions are not shielded enough and protein–ligand electrostatic attractions and repulsions are overestimated, causing the large separation of potent and weak compounds. Other possible enthalpic contributions are related to the lack of thermal effects and protein relaxation/strain as only one structure for each complex is used.

Another potential explanation is associated with the incomplete description of enthalpy–entropy compensation; only the translational, rotational, conformational, and some vibrational entropy changes for the ligand upon binding are included. The important vibrational entropy change associated with the narrowing of the torsional energy wells for the ligands when in the protein

environment is ignored due to its high computational cost. More flexible ligands, which have the opportunity to maximize their interactions with the protein, should pay a more significant torsional entropy penalty due to restriction of their torsional motions.³³ Also ignored are all entropic contributions associated with the protein due to the complexity in computing them.

To evaluate the origin of the large dynamic range in MM-GB/SA, a computational Van't Hoff analysis was conducted for the $H \rightarrow 4\text{-Cl}$ and $H \rightarrow 4\text{-NH}_2$ pairs of ligands by running FEP simulations with MCPRO+ and Desmond at 298 K and at ± 30 K. In the analysis, it was assumed that the heat capacity remains unchanged over the temperature interval.³⁴ The analogs were chosen for two reasons: (1) to save computational time since they are symmetrical like the unsubstituted analog and (2) because the difference in polarity between Cl and NH₂ could provide a more complete picture of the impact of sampling on the theoretical dynamic range. The assumption here is that the results obtained with MCPRO+, with its restricted sampling, can be extrapolated to MM-GB/SA. As can be seen in Figure 6, MCPRO+ is also plagued by a large dynamic range, although to a lesser extent than MM-GB/SA; the value for MCPRO+ is ~ 7.5 kcal/mol, which is more than double the value for Desmond (~ 3.5 kcal/mol). In MCPRO+, only the side chains of residues with any atom within 10 Å from the ligands are varied, and the protein backbone is fixed. Although the ligand is free to move in the unbound state, one should not expect that all accessible conformations and the full range of dihedral angle values for each torsional well are visited, even for very long simulations. This implies that the description of entropic contributions, shielding of electrostatic interactions, thermal effects, and protein relaxation/strain will be somewhat incomplete in the FEP results obtained with MCPRO+.

Table 4. Enthalpic and Entropic Contributions Extracted from Van't Hoff Plots Obtained with MCPRO+ and Desmond (values in kcal/mol)

| | H \rightarrow 4-Cl | | | H \rightarrow 4-NH ₂ | | |
|-----------------------|--------------------------------|----------------------------------|--------------------------------|-----------------------------------|----------------------------------|--------------------------------|
| | $\Delta\Delta H_{\text{bind}}$ | $-T\Delta\Delta S_{\text{bind}}$ | $\Delta\Delta G_{\text{bind}}$ | $\Delta\Delta H_{\text{bind}}$ | $-T\Delta\Delta S_{\text{bind}}$ | $\Delta\Delta G_{\text{bind}}$ |
| MM-GB/SA ^a | | | -4.50 | | | +2.93 |
| MCPRO+ | -4.52 \pm 0.19 | +0.97 \pm 0.24 | -3.55 \pm 0.12 | -8.10 \pm 0.14 | +8.06 \pm 0.17 | -0.04 \pm 0.09 |
| Desmond | -2.52 \pm 0.26 | +1.28 \pm 0.30 | -1.24 \pm 0.15 | -4.53 \pm 0.20 | +4.43 \pm 0.23 | -0.10 \pm 0.12 |
| ITC ^b | -0.29 | -0.76 | -1.05 (-0.78) ^c | +0.99 | -0.49 | +0.50 (-0.05) ^c |

^a MM-GB/SA scoring using eq 5 + RRHO + $E_{\text{GB}} + \Delta G_{\text{solv}}^{\text{ptn}}$. ^b ITC $\Delta\Delta H_{\text{bind}}$ and $-T\Delta\Delta S_{\text{bind}}$ values may be found in ref 18. ^c Values in parentheses were corrected by the equation: $c\Delta G_{\text{bind}} = \Delta G_{\text{bind}} - RT \ln(1 + 10^{(pK_a - pH)})$.

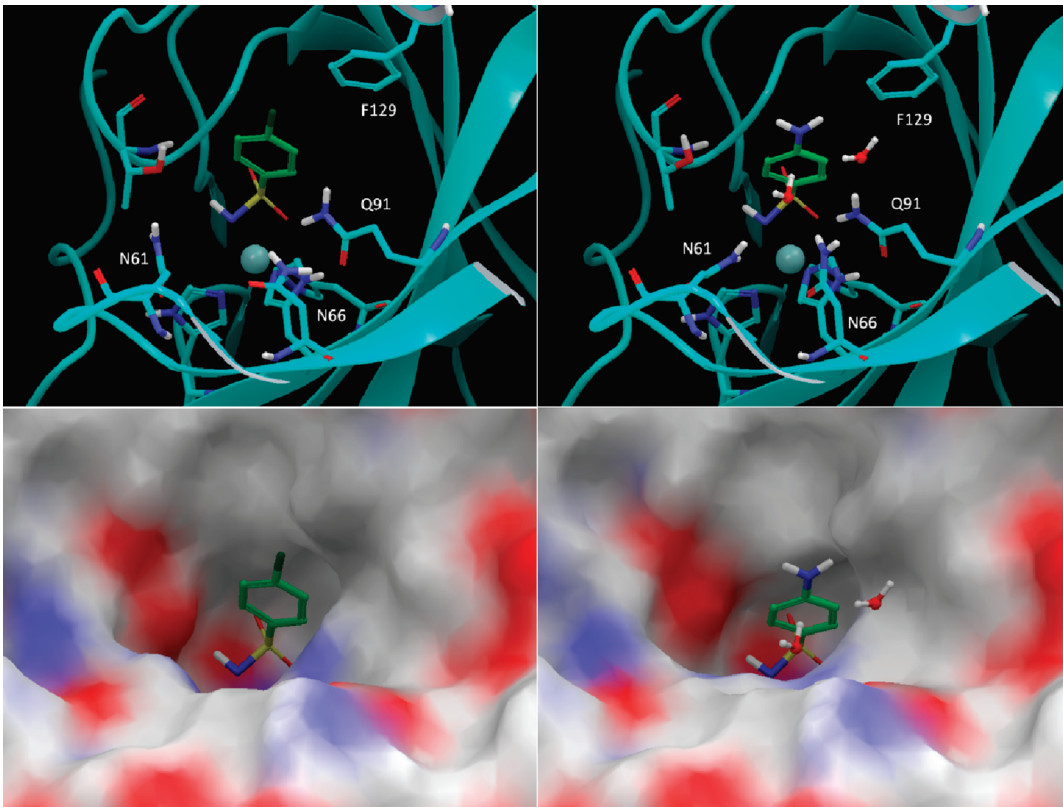
**Figure 10.** Representative theoretical structures of the complexes between human carbonic anhydrase (hCAII) and the 4-Cl (left) and 4-NH₂ (right) substituted benzene sulfonamide inhibitors. Molecular surface representations are also shown at the bottom.

Figure 9 compares the Van't Hoff plots for the H \rightarrow 4-Cl and H \rightarrow 4-NH₂ pairs obtained with Desmond and MCPRO+. The experimental and calculated enthalpic and entropic contributions to the relative binding free energies are shown in Table 4. Although the $\Delta\Delta G_{\text{bind}}$ values obtained with MCPRO+ and Desmond match the experimental values reasonably well, the enthalpic and entropic contributions do not agree with the ITC data. A possible explanation is that, of the parameters measured directly by ITC, the free energy (ΔG^0) has the lowest signal-to-noise ratio, as measured values fall in a relatively narrow range. The enthalpic contribution (ΔH^0) has a higher signal-to-noise ratio, with the entropic contribution (ΔS^0) being even less precise since errors are compounded; ΔS^0 is calculated as the difference between ΔH^0 and ΔG^0 . Alternatively, it is possible that the lack of agreement is due to the fact that the experimental

$\Delta\Delta H_{\text{bind}}$ and $-T\Delta\Delta S_{\text{bind}}$ values still contain the ionization step for the inhibitor before binding to hCAII.

If the analysis is focused on the difference between the FEP methods, it is clear that MCPRO+ provides enthalpic contributions that are exaggerated compared to those from Desmond. In the case of H \rightarrow 4-Cl, it is unlikely that this is due to diminished shielding of electrostatic interaction between the 4-Cl analog and the protein; the substituent is in close contact with a Phe residue (F129; Figure 10). More plausible explanations are either associated with reduced thermal effects that might lead to too favorable VDW interactions and/or limited protein deformation that does not offset the gain in interactions for 4-Cl due to restriction of degrees of freedom in the MC simulations.

It is interesting to see that the MCPRO+ $\Delta\Delta H_{\text{bind}}$ between H and 4-Cl matches their MM-GB/SA relative score of -4.50 kcal/mol,

which despite a few entropic contributions included, is mostly dominated by enthalpic terms. A more significant entropy loss of +0.97 kcal/mol for the 4-Cl derivative compared to the unsubstituted analog results in a $\Delta\Delta G_{\text{bind}}$ of -3.55 kcal/mol obtained with MCPRO+. The increased sampling in Desmond generates a $-T\Delta\Delta S_{\text{bind}}$ value of +1.28 kcal/mol, just slightly more positive than the value reported by MCPRO+ (Table 4). Thus, the larger free energy gap for the H \rightarrow 4-Cl transformation caused by restricted sampling is almost purely enthalpic.

A somewhat different scenario is seen for the H \rightarrow 4-NH₂ pair. Table 4 shows that $\Delta\Delta H_{\text{bind}}$ obtained with MCPRO+ is also exaggerated when compared to Desmond, but differently from the H \rightarrow 4-Cl case, the $-T\Delta\Delta S_{\text{bind}}$ contribution completely offsets that. $-T\Delta\Delta S_{\text{bind}}$ values of +8.06 and +4.43 kcal/mol obtained with MCPRO+ and Desmond, respectively, lead to almost identical $\Delta\Delta G_{\text{bind}}$'s. Figure 10 sheds some light on the enthalpy–entropy compensation observed for the 4-NH₂ analog. It shows that the NH₂ group has the ability to interact with Asn61, Asn66, and Gln91 via water-mediated hydrogen bonds. It is then plausible that in this case the enthalpic and entropic contributions are affected by the different structural and thermodynamic properties of the water molecules in the binding site as a result of restricted versus full protein sampling. A less mobile protein and, consequently, less mobile water molecules in MCPRO+ lead to overly favorable electrostatic interactions for the 4-NH₂ analog due to reduced shielding and thermal effects. The less fluid hydrogen bond network for the 4-NH₂ analog would also result in a greater entropy loss upon binding estimated by MCPRO+. The results obtained with the MC and MD simulations in explicit solvent also explain why the MM-GB/SA relative score for the H \rightarrow 4-NH₂ pair underpredicts the binding energy of the latter; the continuum solvation model is unable to describe the water-mediated hydrogen bonds with the protein that contribute to the binding of the 4-NH₂ analog.

If the implications of MCPRO+ restricted sampling on enthalpic and entropic contributions to binding are extrapolated to MM-GB/SA, a reasonable hypothesis for the large dynamic range in MM-GB/SA is obtained. The scoring spread is not only affected by ignored entropic contributions, i.e., all for the protein and the torsional entropy changes for the ligand, but also exaggerated enthalpic separation between the weak and potent compounds due to the lack of sampling. The resolution of whether this is caused by diminished shielding of electrostatic interactions, thermal effects, or protein relaxation/strain is complex, especially because it seems to be dependent on the case.

CONCLUSIONS

In this work, a series of 13 benzene sulfonamide inhibitors of carbonic anhydrase with binding free energies determined by isothermal titration calorimetry was selected to address whether the MM-GB/SA scoring procedure provides a more attractive alternative for rank-ordering than the more rigorous free energy perturbation (FEP) methodology. In spite of successful applications to elucidate the structure–activity relationships for few pairs of ligands, FEP calculations have rarely been evaluated for more than a handful of compounds. R^2 values of 0.70, 0.71, and 0.49 with the experiment were obtained with MM-GB/SA and FEP simulations run with MCPRO+ and Desmond, respectively, when one outlier (3-Cl derivative) was removed. The main contrast between the methods is the level of sampling, ranging from full to restricted flexibility to single conformation for the

complexes in Desmond, MCPRO+, and MM-GB/SA. All methods work well, but the results obtained with Desmond are inferior to MM-GB/SA and MCPRO+, suggesting that the full flexibility for the complexes in the former leads to additional noise, possibly due to the sampling of nonrelevant conformations and/or relevant conformations that are not adequately weighted in the simulations. In other words, when ranking congeneric series, it is safer to assume that some contributions to binding are roughly constant, and cancel when computing $\Delta\Delta G_{\text{bind}}$, than to actually try to include all of them through full sampling in simulations that are not extremely long.

Regarding the large theoretical dynamic range for the binding energies, that seems to be a direct result of the degree of sampling in the simulations since MCPRO+ as well as MM-GB/SA are plagued by this. Van't Hoff analysis for selected pairs of ligands suggests that the wider scoring spread is not only affected by missing entropic contributions due to restricted sampling but also exaggerated enthalpic separation between the weak and potent compounds caused by diminished shielding of electrostatic interactions, thermal effects, and protein relaxation/strain. Finally, the current and historical results obtained with MM-GB/SA qualify this approach as a more attractive alternative for rank-ordering than the FEP methodology; it can achieve equivalent or superior predictive accuracy and handle more structurally dissimilar ligands at a fraction of the computational cost.

AUTHOR INFORMATION

Corresponding Author

*Phone: (860) 686-2915. E-mail: cristiano.guimaraes@pfizer.com.

ACKNOWLEDGMENT

The author thanks Alan Mathiowetz from Pfizer, Inc. and Robert Abel from Schrodinger, Inc. for helpful discussions.

REFERENCES

- (1) Jorgensen, W. L. Free energy changes in solution. In *Encyclopedia of Computational Chemistry*; Schleyer, P. v. R., Ed.; Wiley: New York, 1998; Vol. 2, pp 1061–1070.
- (2) Kollman, P. A. Free energy calculations: Applications to chemical and biochemical phenomena. *Chem. Rev.* **1993**, *93*, 2395–2417.
- (3) Jorgensen, W. L. Free energy calculations: A breakthrough for modeling organic chemistry in solution. *Acc. Chem. Res.* **1989**, *22*, 184–189.
- (4) Simonson, T.; Georgios, A.; Karplus, M. Free energy simulations come of age: Protein-ligand recognition. *Acc. Chem. Res.* **2002**, *35*, 430–437.
- (5) Guimaraes, C. R. W.; Boger, D. L.; Jorgensen, W. L. Elucidation of fatty acid amide hydrolase inhibition by potent α -ketoheterocycle derivatives from Monte Carlo simulations. *J. Am. Chem. Soc.* **2005**, *127*, 17377–17384.
- (6) Michel, J.; Tirado-Rives, J.; Jorgensen, W. L. Energetics of displacing water molecules from protein binding sites: Consequences for ligand optimization. *J. Am. Chem. Soc.* **2009**, *131*, 15403–15411.
- (7) Michel, J.; Foloppe, N.; Essex, J. W. Rigorous free energy calculations in structure-based drug design. *Mol. Inf.* **2010**, *29*, 570–578.
- (8) Williams, D. H.; Stephens, E.; O'Brien, D. P.; Zhou, M. Understanding noncovalent interactions: Ligand binding energy and catalytic efficiency from ligand-induced reductions in motion with receptors and enzymes. *Angew. Chem., Int. Ed.* **2004**, *43*, 6596–6616.
- (9) (a) Pearlman, D. A.; Charifson, P. S. Are free energy calculations useful in practice? A comparison with rapid scoring functions for the p38

- MAP kinase protein system. *J. Med. Chem.* **2001**, *44*, 3417–3423. (b) Luccarelli, J.; Michel, J.; Tirado-Rives, J.; Jorgensen, W. L. Effects of water placement on predictions of binding affinities for p38alpha MAP kinase. *J. Chem. Theory Comput.* **2010**, *6*, 3850–3856. (c) Mobley, D. L.; Graves, A. P.; Chodera, J. D.; McReynolds, A. C.; Shoichet, B. K.; Dill, K. A. Predicting absolute ligand binding free energies to a simple model site. *J. Mol. Biol.* **2007**, *371*, 1118–1134. (d) Deng, Y.; Roux, B. Calculation of standard binding free energies: Aromatic molecules in the T4 lysozyme L99A mutant. *J. Chem. Theory Comput.* **2006**, *2*, 1255–1273. (e) Boyce, S. E.; Mobley, D. L.; Rocklin, G. J.; Graves, A. P.; Dill, K. A.; Shoichet, B. K. Predicting ligand binding affinity with alchemical free energy methods in a polar model binding site. *J. Mol. Biol.* **2009**, *394*, 747–763. (f) Michel, J.; Verdonk, M. L.; Essex, J. W. Protein-ligand binding affinity predictions by implicit solvent simulations: A tool for lead optimization? *J. Med. Chem.* **2006**, *49*, 7427–7439. (g) Michel, J.; Essex, J. W. Hit identification and binding mode predictions by rigorous free energy simulations. *J. Med. Chem.* **2008**, *51*, 6654–6664.
- (10) Kuhn, B.; Kollman, P. A. Binding of a diverse set of ligands to Avidin and Streptavidin: An accurate quantitative prediction of their relative affinities by a combination of molecular mechanics and continuum solvent models. *J. Med. Chem.* **2000**, *43*, 3786–3791.
- (11) Still, W. C.; Tempczyk, A.; Hawley, R. C.; Hendrickson, T. Semianalytical treatment of solvation for molecular mechanics and dynamics. *J. Am. Chem. Soc.* **1990**, *112*, 6127–6129.
- (12) (a) Bernacki, K.; Kalyanaraman, C.; Jacobson, M. P. Virtual ligand screening against Escherichia coli dihydrofolate reductase: Improving docking enrichment physics-based methods. *J. Biomol. Screening* **2005**, *10*, 675–681. (b) Huang, N.; Kalyanaraman, C.; Irwin, J. J.; Jacobson, M. P. Physics-based scoring of protein-ligand complexes: Enrichment of known inhibitors in large-scale virtual screening. *J. Chem. Inf. Model.* **2006**, *46*, 243–253. (c) Huang, N.; Kalyanaraman, C.; Bernacki, K.; Jacobson, M. P. Molecular mechanics methods for predicting protein–ligand binding. *Phys. Chem. Chem. Phys.* **2006**, *8*, 5166–5177. (d) Lyne, P. D.; Lamb, M. L.; Saeh, J. C. Accurate prediction of the relative potencies of members of a series of kinase inhibitors using molecular docking and MM-GBSA scoring. *J. Med. Chem.* **2006**, *49*, 4805–4808. (e) Lee, M. R.; Sun, Y. Improving docking accuracy through molecular mechanics generalized Born optimization and scoring. *J. Chem. Theory Comput.* **2007**, *3*, 1106–1119. (f) Huang, N.; Jacobson, M. P. Physics-based methods for studying protein-ligand interactions. *Curr. Opin. Drug Discovery Dev.* **2007**, *10*, 325–331. (g) Foloppe, N.; Hubbard, R. Towards predictive ligand design with free-energy based computational methods? *Curr. Med. Chem.* **2006**, *13*, 3583–3608.
- (13) (a) Barril, X.; Gelpí, J. L.; López, J. M.; Orozco, M.; Luque, F. J. How accurate can molecular dynamics/linear response and Poisson–Boltzmann/solvent accessible surface calculations be for predicting relative binding affinities? Acetylcholinesterase Huperine inhibitors as a test case. *Theor. Chem. Acc.* **2001**, *106*, 2–9. (b) Pearlman, D. A. Evaluating the molecular mechanics Poisson-Boltzmann surface area free energy method using a congeneric series of ligands to p38 MAP kinase. *J. Med. Chem.* **2005**, *48*, 7796–807. (c) Kawatkar, S.; Wang, H.; Czerminski, R.; Joseph-McCarthy, D. Virtual fragment screening: An exploration of various docking and scoring protocols for fragments using Glide. *J. Comput.-Aided Mol. Des.* **2009**, *23*, 527–539.
- (14) Guimaraes, C. R. W.; Cardozo, M. MM-GB/SA rescoring of docking poses in structure-based lead optimization. *J. Chem. Inf. Model.* **2008**, *48*, 958–970.
- (15) (a) Friesner, R. A.; Banks, J. L.; Murphy, R. B.; Halgren, T. A.; Klicic, J. J.; Mainz, D. T.; Repasky, M. P.; Knoll, E. H.; Shelley, M.; Perry, J. K.; Shaw, D. E.; Francis, P.; Shenkin, P. S. Glide: A new approach for rapid, accurate docking and scoring. 1. Method and assessment of docking accuracy. *J. Med. Chem.* **2004**, *47*, 1739–1749. (b) Friesner, R. A.; Murphy, R. B.; Repasky, M. P.; Frye, L. L.; Greenwood, J. R.; Halgren, T. A.; Sanschagrin, P. C.; Mainz, D. T. Extra precision Glide: Docking and scoring incorporating a model of hydrophobic enclosure for protein-ligand complexes. *J. Med. Chem.* **2006**, *49*, 6177–6196.
- (16) Guimaraes, C. R. W.; Mathiowitz, A. M. Addressing limitations with the MM-GB/SA scoring procedure using the WaterMap method and free-energy perturbation calculations. *J. Chem. Inf. Model.* **2010**, *50*, 547–559.
- (17) Abel, R.; Young, T.; Farid, R.; Berne, B. J.; Friesner, R. A. Role of the active-site solvent in the thermodynamics of Factor Xa ligand binding. *J. Am. Chem. Soc.* **2008**, *130*, 2817–2831.
- (18) Scott, A. D.; Phillips, C.; Alex, A.; Flocco, M.; Bent, A.; Randall, A.; O'Brien, R.; Damian, L.; Jones, L. H. Thermodynamic optimization in drug discovery: A case study using Carbonic Anhydrase inhibitors. *Chem. Med. Chem.* **2009**, *4*, 1985–1989.
- (19) Jorgensen, W. L.; Maxwell, D. S.; Tirado-Rives, J. Development and testing of OPLS all-atom force field on conformational energetics and properties of organic liquids. *J. Am. Chem. Soc.* **1996**, *118*, 11225–11235.
- (20) Kaminski, G. A.; Friesner, R. A.; Tirado-Rives, J.; Jorgensen, W. J. Evaluation and reparametrization of the OPLS-AA force field for proteins via comparison with accurate quantum chemical calculations on peptides. *J. Phys. Chem. B* **2001**, *105*, 6474–6487.
- (21) Wong, C. F.; McCammon, J. A. Dynamics and design of enzymes and inhibitors. *J. Am. Chem. Soc.* **1986**, *108*, 3830–3832.
- (22) MCPRO+, version 1.36; Schrödinger, LLC: New York, 2008.
- (23) Desmond, version 2.2; Schrödinger, LLC: New York, 2009.
- (24) Anderson, H. C. Rattle: A ‘velocity’ version of the Shake algorithm for molecular dynamics simulation. *J. Comput. Phys.* **1983**, *52*, 24–34.
- (25) Essman, U.; Perera, L.; Berkowitz, M. L.; Darden, T.; Lee, H.; Pedersen, L. G. A smooth particle mesh Ewald method. *J. Chem. Phys.* **1995**, *103*, 8577–8593.
- (26) Bennett, C. H. Efficient estimation of free energy differences from Monte Carlo data. *J. Comput. Phys.* **1976**, *22*, 245–268.
- (27) Beutler, T.; Mark, A.; van Schaik, R.; Gerber, P.; van Gunsteren, W. Avoiding singularities and numerical instabilities in free energy calculations based on molecular simulations. *Chem. Phys. Lett.* **1994**, *222*, 529–539.
- (28) Berendsen, H. J. C.; Postma, J. P. M.; Van Gunsteren, W.; Dinola, A.; Haak, J. R. Molecular-Dynamics with coupling to an external bath. *J. Chem. Phys.* **1984**, *81*, 3684–3690.
- (29) Jorgensen, W. L.; Chandrasekhar, J.; Madura, J. D.; Impey, W.; Klein, M. L. Comparison of simple potential functions for simulating liquid water. *J. Chem. Phys.* **1983**, *79*, 926–935.
- (30) Berendsen, H. J. C.; Grigera, J. R.; Straatsma, T. P. The missing term in effective pair potentials. *J. Phys. Chem.* **1987**, *91*, 6269–6271.
- (31) MacroModel, version 9.0; Schrödinger, LLC: New York, 2005.
- (32) WaterMap, version 1.0; Schrödinger, LLC: New York, 2008.
- (33) Chang, C. A.; Chen, W.; Gilson, M. K. Ligand configurational entropy and protein binding. *Proc. Natl. Acad. Sci. U.S.A.* **2007**, *104*, 1534–1539.
- (34) Prabhu, N. V.; Sharp, K. A. Heat capacity in proteins. *Annu. Rev. Phys. Chem.* **2005**, *56*, 521–548.